





Net Radiation in the Semiarid Region of the States of Paraíba and Rio Grande do Norte Using the MODIS Sensor

Balanco de Radiação na Região Semiárida dos Estados da Paraíba e Rio Grande do Norte Utilizando o Sensor MODIS

Madson Tavares Silva¹ , Verônica Gabriella de Oliveira¹ ,
Carlos Antonio Costa dos Santos¹ , Lindenberglucena da Silva¹ ,
Francineide Amorim Costa Santos² , Edivaldo Afonso de Oliveira Serrão¹ 

¹Universidade Federal de Campina Grande, Programa de Pós-Graduação em Meteorologia, Campina Grande, PB, Brasil.

²Universidade Federal do Cariri, Brejo Santo, CE, Brasil.

Emails: madson.tavares@ufcg.edu.br; oliver.gabzinha@hotmail.com; carlostorm@gmail.com; begapb@gmail.com; francineide.amorim@ufca.edu.br; oliveiraserrao@gmail.com

Corresponding author: Madson Tavares Silva; madson.tavares@ufcg.edu.br

Abstract

This study aims to estimate the surface net radiation (R_n) in experimental areas in the States of Paraíba and Rio Grande do Norte, as well as to validate the results with data measured in areas with Caatinga patterns in recovery (CRec), degraded (CDeg) and preserved (CPres). Seventeen images from the MODIS sensor aboard the Terra satellite were selected for CRec and CDeg in the State of Paraíba and twenty-eight images for the CPres in Rio Grande do Norte corresponding to the period from January to December 2014. MODIS/Terra MOD09A1 and MOD11A2 products to obtain the albedo, temperature, and surface radiation balance. Parametric (Shapiro-Wilk) and non-parametric (Kolmogorov-Smirnov and Wilcoxon-Mann-Whitney) tests were applied to understand the distribution patterns of the variables. Statistical error indices were applied to verify the accuracy of the estimates in relation to the observed values. Only the measured albedo (α_{meas}) did not meet the normality assumption in the three study areas. According to the absolute mean percentage error statistic, the model used to estimate the albedo was classified as inappropriate for CPres and CRec (> 25%), while it was satisfactory for CDeg (15-25%). Significant differences between observed and estimated values were absent only for R_n in the three observation sites. Therefore, we conclude that the R_n estimates obtained by processing orbital data were satisfactory for the three Caatinga coverage areas. These results are significant and can be used as tools for monitoring the process of surface energy exchange in semiarid regions.

Keywords: Remote sensing; Albedo; Caatinga

Resumo

Este estudo teve como objetivo estimar a radiação líquida superficial (R_n) em áreas experimentais nos Estados da Paraíba e Rio Grande do Norte, como também validar os resultados com dados medidos em áreas com padrões de Caatinga em recuperação (CRec), degradada (CDeg) e preservada (CPres). Foram selecionadas dezessete imagens do sensor MODIS a bordo do satélite Terra para o CRec e CDeg no Estado da Paraíba e vinte e oito imagens para os CPres no Estado do Rio Grande do Norte, correspondentes ao período de janeiro a dezembro de 2014. Foram usados os produtos MODIS/Terra MOD09A1 e MOD11A2, para obtenção do albedo, temperatura e saldo de radiação à superfície. Testes paramétricos (Shapiro-Wilk) e não paramétricos (Kolmogorov-Smirnov e Wilcoxon-Mann-Whitney) foram aplicados para a compreensão dos padrões de distribuição das variáveis. Índices de erros estatísticos foram aplicados para verificar a precisão das estimativas em relação aos valores observados. Apenas o albedo medido (α_{meas}) não atendeu ao pressuposto de normalidade nas três áreas de estudo. De acordo com a estatística do erro percentual médio absoluto, o modelo utilizado para estimar o albedo foi classificado como impróprio para CPres e CRec (> 25%), enquanto foi satisfatório para CDeg (15-25%). Diferenças significativas entre os valores observados e estimados estavam ausentes apenas para a variável R_n nos três locais de observação. Portanto, concluímos que as estimativas de R_n obtidas pelo processamento de dados orbitais foram satisfatórias para as três áreas de cobertura de Caatinga. Esses resultados são significativos e podem ser usados como ferramentas de monitoramento do processo de trocas de energia à superfície em regiões semiáridas.

Palavras-chave: Sensoriamento remoto; Albedo; Caatinga

Received: 29 March 2021; Accepted: 05 October 2021

Anu. Inst. Geociênc., 2022;45:42790

DOI: https://doi.org/10.11137/1982-3908_45_42790 1

1 Introduction

Net radiation (R_n) is the electromagnetic energy available at the Earth's surface that regulates most physical and biological processes, such as evapotranspiration (Lu et al. 2013), photosynthesis, turbulent flows, and heat conduction fluxes (Jiang et al. 2015). Therefore, accurate estimates of R_n are essential for understanding the distribution of energy on the Earth's surface, formation and transformation of air masses, melting, as well as for agrometeorological modeling and water resource management (Bisht & Bras 2011; Hwang et al. 2013), thus being a critical component in agricultural, hydrological, ecological, and climatic research (Amatya et al. 2015; Jiang et al. 2015).

Net radiation is the difference between incoming and reflected shortwave radiation (SW) and incoming and outgoing longwave radiation (LW) fluxes on the Earth's surface. Net radiation values are usually positive during the daytime when net shortwave radiation is dominant but negative at nighttime when net longwave radiation predominates (Allen et al. 1998). Thus, estimating R_n is fundamental for understanding the climate in the lower layers of the atmosphere. It depends on the structure and composition of the adjacent atmosphere and the presence of clouds and surface characteristics, such as albedo, emissivity, temperature, humidity, and thermal properties of the soil (Cueto et al. 2015).

Accurate measures of R_n , which are essential for understanding the physical and biological processes of evapotranspiration and air and soil heating, are obtained with net radiometers installed on the surface (direct measurements). However, these instruments are expensive, require frequent calibration, and have limited spatial distribution. Thus, several models have been developed to estimate R_n through conventional meteorological parameters (Mahalakshmi et al. 2016). In addition, to obtain the spatial and temporal distribution of the components of R_n , studies have been developed with algorithms making use of orbital remote sensing products. However, this technique's problems are the frequent cloud cover over certain areas, which directly interferes with R_n estimates using satellite data (Liang et al. 2010; Santos et al. 2017; Santos et al. 2020).

Under the cloudy condition, the visible (VIS) and infrared (IR) imagers cannot sense surface properties as the albedo and temperature over a pixel, and it only could be achieved using other remote sensing techniques, such as microwave. On the other hand, many studies presented high accurate methodologies to estimate components of the SW and LW fluxes under cloudy skies coverage (Pinker et al. 2003; Ceballos et al. 2004; Bisht & Bras 2010, 2011;

Carmona, Rivas & Casseles 2014; Wang et al. 2018; Jiang et al. 2019), and these components could be used to estimate R_n .

The MODIS sensor onboard the National Aeronautics and Space Administration (NASA) Terra and Aqua polar-orbiting satellites provide global coverage with approximately four passes a day. Furthermore, with 36 spectral bands between 0.405 and 14.385 μm and spatial resolution ranging from 250 m to 1 km, MODIS offers products related to the atmosphere, surface, cryosphere, and oceans (Bisht & Bras 2011). These characteristics make it a good option for the study of surface R_n in the semiarid region of Brazil, because of its proximity to the Atlantic Ocean, cloud cover is frequent throughout the day in this region, considerably reducing the possibilities of obtaining cloudless satellite images from satellites with higher spatial resolution and lower temporal resolution, for example, the Landsat satellite with a 16-day orbital cycle (Santos et al. 2017; Santos et al. 2020; Oliveria et al. 2021).

In this context, the assessment of the accuracy of R_n data under clear sky obtained from remote sensing products is necessary, as it has been done in different studies such as those developed by Santos et al. (2013), Santos et al. (2015), Mira et al. (2016), Araújo et al. (2017), Araújo et al. (2018), Santos et al. (2017), and Santos et al. (2020). For that, estimates using remote sensing data were compared with surface R_n measures in experimental areas. However, few studies have been developed to understand space/time behavior of R_n in the semiarid region of Brazil, particularly in the Caatinga ecosystem.

The objective of this study was to estimate R_n under a clear sky for the states of Paraíba and Rio Grande do Norte based on MODIS sensor data and validate the results with measurements in experimental recovering (CRec), degraded (CDeg), and preserved (CPres) areas of Caatinga, the predominant vegetation in the territory of these states and which has undergone a continuous and intense degradation process.

2 Material and Methods

2.1 Description of the Study Area and Analyzed Period

The study was conducted in semiarid areas of the states of Paraíba and Rio Grande do Norte (Figure 1), and the period selected was the year 2014. According to Alvares et al. (2014), according to the Köppen classification, the semiarid climate (type BSh) is characteristic of NEB, where annual precipitation is less than 800 mm, where B represents the dry climate zone, semiarid Bs and BSh

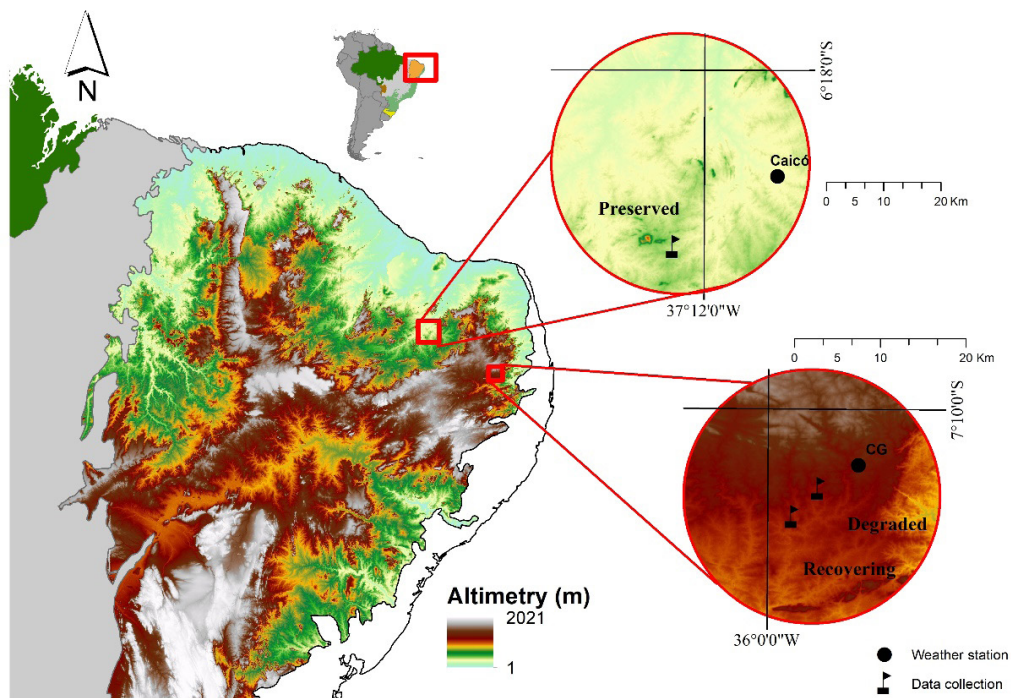


Figure 1 Location of the states of Paraíba and Rio Grande do Norte. Arrows indicate the locations of the three micrometeorological towers and INMET meteorological stations.

for low latitude and altitude. In the Borborema Plateau, in Paraíba. The average annual air temperature varies between 21.5 and 26 °C, and the relative air humidity is around 60% (Francisco et al. 2015). The main rainfall production mechanisms in the study region are the frontal systems, the intertropical convergence zone (ITCZ), and wave disturbances in the field of trade winds. According to the studies by Marengo and Bernasconi (2015), Marengo et al. (2017) and Marengo et al. (2018), the 2012-2016 time frame was verified as the most severe dry period of all times recorded in the Brazilian semiarid region.

2.2 Data

The analyzes were carried out in two experimental sites belonging to the Instituto Nacional do Semiárido (INSA), located in the municipality of Campina Grande - PB, which were classified as: 1) degraded Caatinga (CDeg) - located near the administrative headquarters of INSA (7°14'59" S, 35°56'49" W) (Figure 1). The soil characteristics are sandy sediments with the occurrence of some ravines; 2) Caatinga in recovery (CRec) - located in the experimental farm of INSA (7°16'47" S; 35°58'29" W) (Figure 1).

The vegetation had a very structured vegetative canopy, predominantly characterized by the presence of a shrub layer, where some scattered arboreal individuals

were observed, in addition to a large concentration of cacti, differing only in their density. The third experimental site called preserved Caatinga (CPres) - a preserved fragment of a dry tropical forest (6°34'42" S, 37°15'05" W), is located at the Seridó Ecological Station (ESEC-Seridó), municipality of Serra Negra do Norte, in the state of Rio Grande do Norte (Figure 1). ESEC-Seridó comprises an area of 1163 ha of Caatinga remnant, characterized by dry xerophilous forest and deciduous plant species and the predominance of small, widely dispersed trees and shrubs less than 7 m tall and patches of grass, which develop and grow only during the rainy season (Tavares-Damasceno et al. 2017). The climate of the region is semiarid, the low longitude and altitude of the Köppen Bsh (Alvares et al. 2014), with the rainy season occurring between January and May, average annual precipitation of 700 mm, average annual temperature of 25 °C and average annual air humidity around 60% (average of 30 years).

MODIS/Terra data were acquired through the Reverb platform (<http://reverb.echo.nasa.gov/>) made available by the EOSDIS (Earth Observing System Data and Information System) agency belonging to NASA (<https://earthdata.nasa.gov/>). The MODIS products used in this study is provided in Table 1. For the formation of the mosaic of images that contain the study area was used the Tile h13v09.

Table 1 Description of MODIS products used in this study.

| Product | Description | Multip. Factor | Addit. Factor | Resolution (spatial and temporal) | Units |
|---------|----------------------------------|----------------|---------------|-----------------------------------|---------------|
| MOD11A2 | Surface temperature | 0.02 | - | - | Kelvin |
| | Emissivity of bands 31 and 32 | 0.002 | 0.490 | 1000 m 8 days | Dimensionless |
| | Satellite pass time | 0.1 | - | - | Hour |
| MOD09A1 | Surface reflectance | 0.0001 | - | 500 m 8 days | Kelvin |
| | Solar zenith angle | 0.01 | - | 1000 m 8 days | degree |
| | Sequential day of the year (SDY) | - | - | 1000 m 8 days | Julian day |

Source: <http://modis.gsfc.nasa.gov/>

Rainfall data for Campina Grande-PB and Caicó-RN (Figure 1) were obtained from the BDMEP (Meteorological Database for Teaching and Research) of the INMET - National Institute of Meteorology (<http://www.inmet.gov.br/portal/index.php?r=bdmep/bdmep>).

2.3 Data Processing

Net radiation at the moment of passage of the MODIS sensor was estimated as described in Equation 1.

$$R_n = R_{S\downarrow} - \alpha R_{S\downarrow} + R_{L\downarrow} - R_{L\uparrow} - (1 - \epsilon_0) R_{L\downarrow} \quad (1)$$

where: R_n is the net radiation (Wm^{-2}), $R_{S\downarrow}$ is the incoming shortwave radiation (Wm^{-2}); α is the surface albedo (dimensionless); $R_{L\downarrow}$ is the incoming longwave radiation to the atmosphere (Wm^{-2}); and $R_{L\uparrow}$ is the longwave radiation emitted by the surface to space (Wm^{-2}); and ϵ_0 is the surface thermal emissivity (dimensionless). The term $(1-\epsilon_0) R_{L\downarrow}$ represents the fraction of incoming longwave radiation reflected by the surface.

As direct and diffuse radiation at the Earth's surface, represents the main source of energy for evapotranspiration (ET) and was estimated from Equation 2:

$$R_{S\downarrow} = \frac{G_{sc} \cdot \cos\theta_{hor} \cdot \tau_{sw}}{d^2} \quad (2)$$

In this equation, G_{sc} is the solar constant ($1367 W m^{-2}$), θ_{hor} is the solar zenith angle for the horizontal surface obtained through the MOD09 product band, d^2 is the square of the relative distance between Earth and Sun; and τ_{sw} is the atmospheric transmissivity (dimensionless).

Transmissivity (τ) was calculated according to Equation 3 simply with the aid of the digital elevation model (DEM), as proposed by Allen et al. (2002):

$$\tau_{sw} = 0,75 + 2 \cdot 10^{-5}z \quad (3)$$

where: z represents the altitude of each pixel, obtained from the DEM, generated by SRTM (Shuttle Radar Topography Mission), from <http://www.relevobr.cnpm.embrapa.br/conteudo/relevo/metodo.htm>.

The parameter d^2 (relative distance between Earth and Sun) was calculated as a function of the sequential day of the year (DOY) using Equation 4, as proposed by Duffie and Beckman (1991):

$$d^2 = \frac{1}{1 + 0,033\cos(DOY \cdot 2\pi/365)} \quad (4)$$

where: DOY value for each pixel from the MOD09A1 product was used in the calculation.

Surface albedo (α) was calculated according to the methodology described in Tasumi et al. (2008) using Equation 5:

$$\alpha\tau = \sum_{b=1}^n (p_{s,b} w_b) \quad (5)$$

where: w_b are the weighting coefficients that represent the fraction of solar radiation that occurs in the spectral range of the specific band (see values in Tasumi et al. 2008); n is the corresponding number of bands; and $p_{s,b}$ is the surface spectral reflectance, obtained from the MOD09A product.

The longwave radiation emitted by the surface ($W m^{-2}$) was obtained from the surface temperature and emissivity, calculated according to Equation 6 as proposed by the Stefan-Boltzmann law:

$$R_{L\uparrow} = \sigma \epsilon_0 T_s^4 \tag{6}$$

where: σ is the Stefan-Boltzmann constant ($5.67 \times 10^{-8} W m^{-2} K^{-4}$), ϵ_0 is the surface emissivity, and T_s (K) represents the surface temperature obtained from the MOD11 product that provides daily data on Earth's surface temperature. Surface emissivity was considered equal to the arithmetic mean of bands 31 and 32, available in the MOD11A2 product, as Bisht et al. (2005) proposed.

The incoming longwave radiation ($R_{L\downarrow}$) was estimated from Equation 7 as proposed by Stefan-Boltzmann:

$$R_{L\downarrow} = \epsilon_a \sigma T_a^4 \tag{7}$$

where: ϵ_a is the atmospheric emissivity; σ is the Stefan-Boltzmann constant ($\sigma = 5.67 \times 10^{-8} W m^{-2} K^{-4}$); and T_a is the near-surface air temperature.

The term $R_{L\downarrow}$ was estimated according to the method used by Araújo et al. (2017). The proposal is that the surface temperature T_s of each pixel of the image can be used in place of T_a , suggesting that $R_{L\downarrow}$ varies proportionally to T_s . In other applications, a fixed value of T_a can be used for the entire scene, considering constant throughout the image in this case, with T_a equal to the T_s of the cold pixel (Araújo et al. 2012).

In order to estimate $R_{L\downarrow}$, the Equation 8 was used, as proposed by Bastiaanssen (1995), and the coefficients proposed by Araújo et al. (2012) were used for the NEB, which are:

$$\epsilon_a = 0,9565(-\ln \tau_{sw})^{0,1362} \tag{8}$$

2.4 Statistical Analysis

2.4.1. Statistical Tests

Remote sensing estimates were validated using the ground database, but first, the probability distribution of these two datasets was analyzed, applying three hypothesis testing, as described below. Some tests can be applied to check the normality of the observed and estimated values. According to Royston (1983), the Shapiro-Wilk test stands out as the option for checking the normality of the values of environmental variables. The Kolmogorov-Smirnov (KS) test was also applied, considering that the traditional parametric tests based on the t-Student distribution are obtained under the hypothesis that the population has a normal distribution. In this sense, there is a need to make sure whether this assumption can be made. Finally, to test whether the distributions of the observed and estimated variables were equal in location, that is, whether one population tended to have higher values than the other or whether they had the same median, we used the non-parametric Wilcoxon-Mann-Whitney test. The tests used are summarized in Table 2. The significance level adopted in all tests was 0.05.

2.4.2. Error Statistics

In order to check the accuracy of the estimated values in relation to the observed values, it was necessary to investigate the following error estimation methods.

Absolute Error (AE) is the difference between the measured and the actual values. It is a way of considering the error when measuring the precision of the values, obtained by Equation 9:

$$AE = E_i - O_i \tag{9}$$

Table 2 Tests used and their respective hypotheses.

Shapiro-Wilk test

H_0 : sample comes from a normally distributed population.
 H_1 : sample does not come from a normally distributed population.
 Decision making: if the p-value is greater than α , that is, $p > 0.05$; (do not reject H_0).

Kolmogorov-Smirnov test

H_0 : The distribution of the two samples is the same.
 H_1 : The distributions of the two samples are different.
 Decision making: if the p-value is greater than α , that is, $p > 0.05$; (do not reject H_0).

Wilcoxon - Mann - Whitney test

H_0 : The difference in position between the samples is equal to 0.
 H_1 : The difference in position between samples is different from 0.
 Decision making: if the p-value is greater than α , that is, $p > 0.05$; (do not reject H_0).

The Mean Absolute Error (MAE) estimates the mean error value between the series observed and adjusted according to Equation 10:

$$MAE = \frac{1}{N} \sum_{i=1}^N |E_i - O_i| \tag{10}$$

The Root Mean Square Error (RMSE) represents the individual quadratic differences between the observed and estimated time series obtained from Equation 11:

$$RMSE = \sqrt{\frac{1}{N} \sum_{i=1}^N (E_i - O_i)^2} \tag{11}$$

The Mean Absolute Percentage Error (MAPE) estimates the percentage error. This is calculated as the mean of the percentage error according to Equation 12:

$$MAPE = \frac{1}{N} \sum_{i=1}^N \left| \frac{E_i - O_i}{O_i} \right| \times 100 \tag{12}$$

The Nash-Sutcliffe (NS) efficiency coefficient can vary from $-\infty$ to 1; the value 1 indicates a perfect fit. The expression used to calculate NS is given by Equation 13:

$$NS = 1 - \frac{\sum_{i=1}^N (O_i - E_i)^2}{\sum_{i=1}^N (O_i - \bar{O}_i)^2} \tag{13}$$

The Willmott Index numerically quantifies the accuracy between the differences through a coefficient of agreement obtained by Equation 14:

$$d = 1 - \frac{\sum_{i=1}^N (E_i - O_i)^2}{\sum_{i=1}^N (|E_i - \bar{O}_i| + |O_i - \bar{O}_i|)^2} \tag{14}$$

where: O_i is the value observed in the experimental area, E_i the value estimated through the processing of MODIS products, \bar{O}_i the mean of the observed values, and N the number of observations. The “ d ” values can range from 0, for no agreement, to 1, for perfect agreement. Further details on error statistics can be found in Nash and Sutcliffe (1970), Cochran (1977), and Montgomery et al. (2015).

All calculations and adjustments necessary to carry out this work were performed using scripts from the R software (R Development Core Team 2016). In addition, we used R modules with specific functions for the analysis developed in this research.

3 Results and Discussion

3.1 Analysis of Environmental Variables

The results obtained from the application of the Shapiro-Wilks test to the values of the biophysical variables monitored in the present study are shown in Table 3. The results indicated that, for all soil covers (CRec, CDeg and CPres), the values of the majority of variables showed a normal distribution, except for α_{measured} ; $\alpha_{\text{estimated}}$ -CDeg; $Ts_{\text{(estimated)}}$ -CPres and $Ts_{\text{(measured)}}$ -CRec. The normality pattern is directly associated with the frequency of values obtained, in which there is equality between the mean and the median. This assumption and its association with the values can be explained by the characteristics of short time and space variabilities.

As some variables did not meet the assumption of normality, it was necessary to apply tests of non-parametric nature. The Kolmogorov-Smirnov (KS) statistic was first applied, and then the distance between the cumulative relative frequency distribution curves of measured and estimated albedo values (Figure 2A) was quantified,

Table 3 Shapiro-Wilk statistics at 5% level of significance for the data sample points.

| Locality (Caatinga) | Variable (p-value) | | | | | |
|------------------------|-----------------------------|----------------------------|---------------------------|--------------------------|---------------------------|--------------------------|
| | $\alpha_{\text{estimated}}$ | α_{measured} | $R_{n(\text{estimated})}$ | $R_{n(\text{measured})}$ | $Ts_{\text{(estimated)}}$ | $Ts_{\text{(measured)}}$ |
| Preserved | 0.08 | < 0.001*** | 0.15 | 0.07 | 0.04* | 0.18 |
| Recovering | 0.58 | < 0.02* | 0.70 | 0.48 | 0.33 | 0.02* |
| Degraded | 0.019* | < 0.0001*** | 0.70 | 0.23 | 0.19 | 0.10 |

Significance codes: ***0.001, **0.01, *0.05.

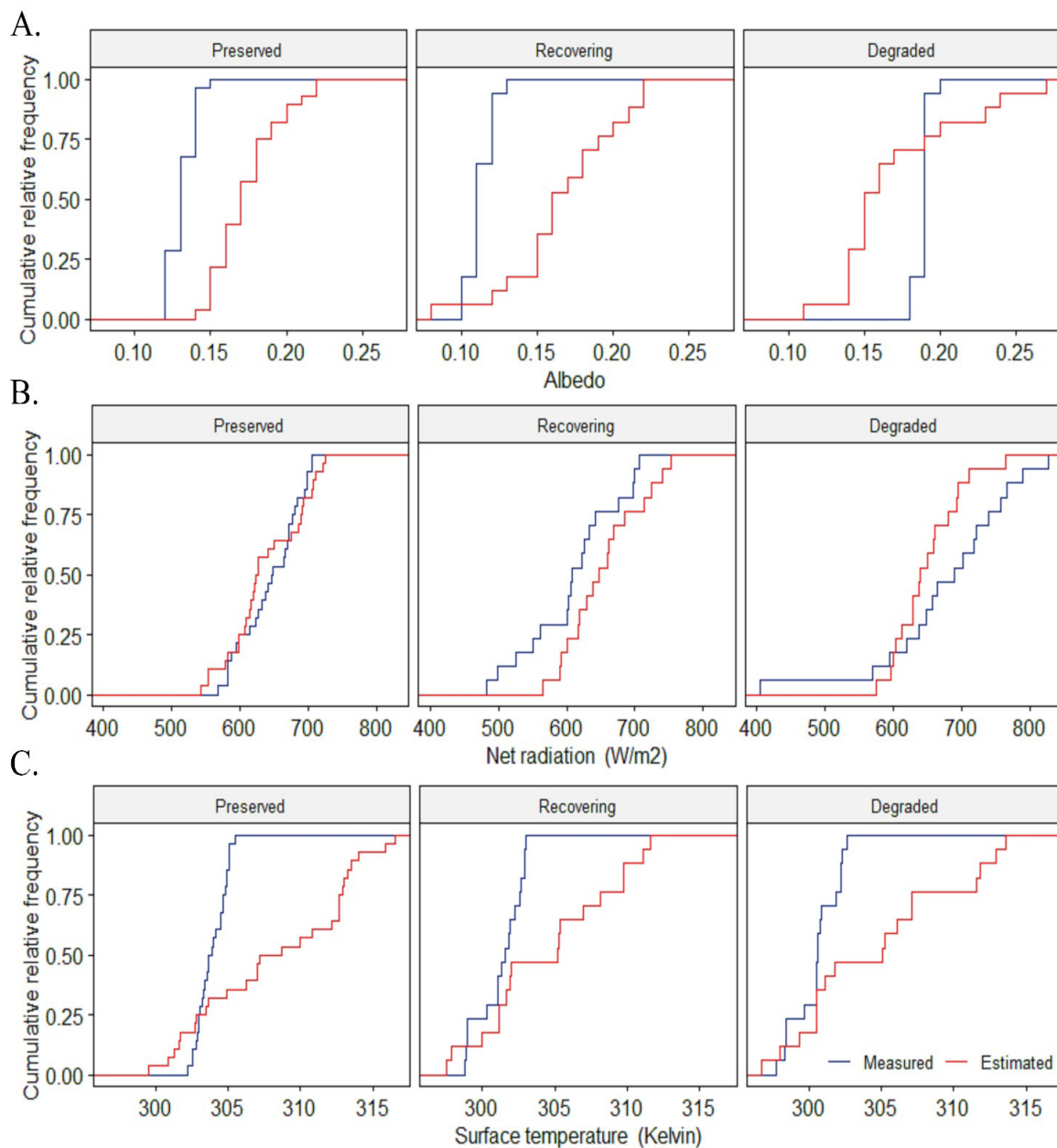


Figure 2 Cumulative relative frequency distribution curves obtained from the KS test for measured (blue line) and estimated (red line) values in the Caatinga preserved (CPres), recovering (CRec) and degraded (CDeg) areas for the period analyzed: A. Albedo; B. Net radiation (Wm⁻²); C. Surface temperature (Kelvin).

resulting in the comparison between the two distributions and computation of the KS test. The results indicated different distributions between the two samples in all three patterns of land use (p -value < 0.0001). However, the results of the KS test applied to net radiation (R_n) did not indicate a difference between the distribution of the two samples (p -value: 0.19-0.39); that is, the cumulative relative frequency patterns were equal for the observed and estimated values (Figure 2B). According to Figure

2B, the best fit between the curves occurred in CPres, which can be explained by maintaining natural soil cover conditions, leading to smaller divergences from the observed values. Such characteristics can be directly associated with seasonal patterns of photosynthetic activity in Caatinga areas without anthropogenic actions; that is, the inexistence of significant changes in the CPres area ensures the maintenance of natural patterns of land cover and use.

The surface temperature variable had p-values ranging from 0.0001 to 0.01 in the KS test, indicating that the two samples had different distributions, that is, different cumulative relative frequency patterns of observed and estimated values (Figure 2C). Furthermore, the distance between the curves of the observed and estimated values can be associated with the pixel size used to calculate the estimated values (pixel = 1 km). Thus, the homogeneity of surface cover patterns can directly influence the satellite’s spectral response.

3.2 Spatio-Temporal Variability of Environmental Variables

Albedo (α), net radiation (R_n), and surface temperature (T_s) estimate based on satellite data (MODIS) and surface measurements (net radiometers) installed at points with different soil cover patterns (preserved, recovering and degraded areas) are shown in Figure 3. The lowest estimated albedo ($\alpha_{estimated}$) value in the recovering (CRec) area was of the order of 0.08, and the highest was of the order of 0.22; these values were recorded in the period without the presence of rainfall or with little soil moisture accumulation on the days that preceded the passage of the satellite (Figure 3A). In general, the data dispersion pattern for this area was associated with the extreme albedo values, possibly explained by the natural process and the dynamics of recovery of soil cover patterns. The minimum and maximum estimated albedo ($\alpha_{estimated}$) values in the degraded (CDeg) area were 0.11 and 0.27, respectively, and the minimum and maximum $\alpha_{measured}$ values were 0.18

and 0.20 (Figure 3A). The highest estimated and measured albedo values were observed in this specific study area compared to the other land cover types (Figure 3A). The differences of absolute error were also the largest in this area (Figure 3B). It was also noticed that $\alpha_{measured}$ presented a more homogeneous pattern in the observations (values close to 0.19). Such variability of α_{MODIS} data may be associated with atmospheric conditions when recording the image and with edaphoclimatic characteristics of the study area.

In degraded areas, uncovered or partially uncovered soils tend to predominate. As a result, a large portion of the Rn fraction is stored on the surface, resulting in a much greater amount of energy in degraded surfaces than in recovering or vegetated surfaces. In this study, there was a pattern of underestimations of albedo based on MODIS images ($\alpha_{estimated}$) in most days in relation to data from the micrometeorological tower ($\alpha_{measured}$) in the degraded area. This fact can be justified by the spatial resolution of the MODIS product, especially if an area is heterogeneous, and also by external factors such as rain before the satellite passage.

Teixeira et al. (2008) found minimum and maximum albedo values, respectively, of 0.11 and 0.17 in the years 2004 and 2005 through field measurements for natural vegetation (Caatinga) in the semiarid zone of the São Francisco River basin (Brazil) in the state of Pernambuco.

Quantitative data of surface $\alpha_{estimated}$ for the domains of CPres showed values from 0.15 to 0.22 (Figure 3A). In turn, the minimum and maximum albedo values measured at the micrometeorological towers were 0.12 and 0.15, respectively. The mean measured ($\alpha_{measured}$) value was of the

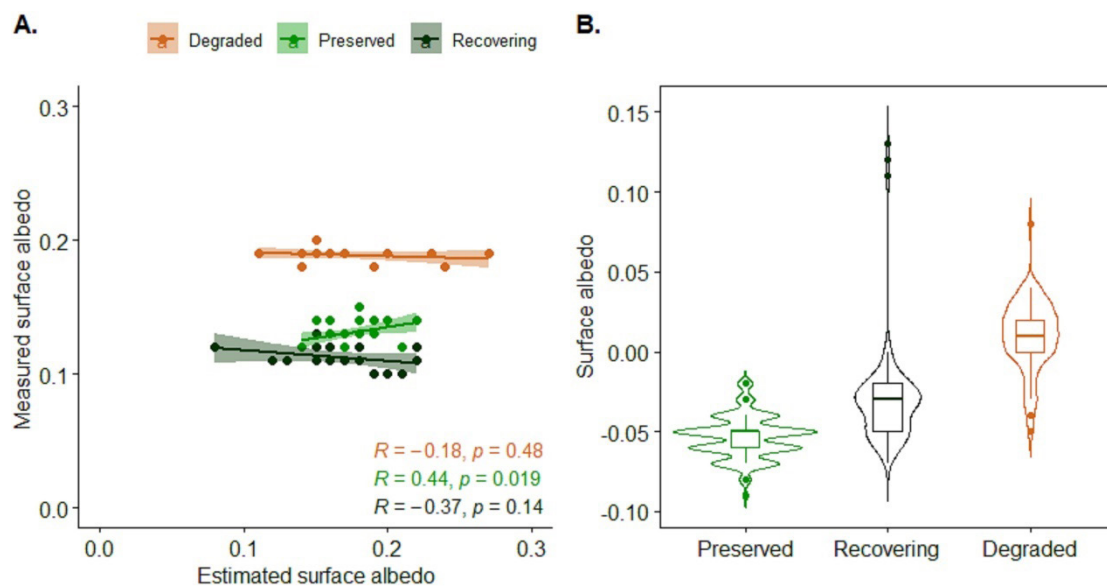


Figure 3 Distribution of measured and estimated: A. Surface albedo values in the studied areas; B. Associated absolute error.

order of 13% and the estimated of 18%, and it was clear that the amplitude of the AE for this locality was the smallest in comparison with the other land cover types (Figure 3B), which may be associated to the vegetation pattern with few spatial changes, making the surface's reflecting capacity remain active during most of the period studied. Santos et al. (2020) evidence that the remote sensing methodology overestimated albedo, which could be due to the inability of the MOD09GA to resolve the land surface heterogeneity of the Caatinga (sparse vegetation).

Regarding the R_n values in CRec, the highest $R_{n(estimated)}$ value recorded was 752.8 W m^{-2} in the summer season, and the highest $R_{n(measured)}$ value was 706.2 W m^{-2} ; the lowest $R_{n(estimated)}$ value was 564.7 W m^{-2} and the lowest $R_{n(measured)}$ value was 483.2 W m^{-2} . It was observed that $R_{n(estimated)}$ values were higher than $R_{n(measured)}$ values (Figure 4A), which can be explained by the fact that 1-km resolution pixels were used, what covered the entire area, including vegetated and exposed soils, while data coming from measurements at the micrometeorological tower covered a radius of about 300 m. In this context, Pigeon et al. (2007) highlights that, in experiments on a local scale, the representativeness of measurements carried out in the tower can be considered a circular perimeter of up to 500 m around the micro-meteorological tower.

In CDeg, the maximum and minimum $R_{n(estimated)}$ values recorded were 792.5 and 596.9 W m^{-2} , respectively. On the other hand, values measured at the micrometeorological towers ranged from 404.2 to 826.4 W m^{-2} . In general, in the analysis of R_n values of the degraded area of Paraíba, it was seen that the estimated R_n was the variable that presented

the highest values for most of the selected days, reflecting an overestimation in relation to $R_{n(measured)}$; the variability of the absolute error (Figure 4B) can be associated with the estimates of the components of $R_{n(estimated)}$, and this could explain the great amplitude between maximum and minimum values.

In CPres, R_n values estimated through MODIS data varied from 542.5 to 722.3 W m^{-2} , and those measured at the micrometeorological tower varied from 568.5 W m^{-2} (corresponding to the rainiest month in this region) to 706.2 W m^{-2} (corresponding to the dry season). The variability of R_n values estimated through remote sensing data was close to 180 W m^{-2} during the period studied, showing an interval between the minimum and maximum values much higher than that (137.7 W m^{-2}) of values measured at the tower.

Rainfall forcing can explain the deviations in the quantitative assessment of surface R_n in both cases $R_{n(estimated)}$ and $R_{n(measured)}$. In the case of CPres, precipitation data (Figure 5A) from the INMET station in Caicó-RN, at a distance of 22 km from the micrometeorological tower of CPres, showed that all image records after the SDY 151 (May 31) were made practically for dry days, with just over 10 mm only in the SDY 178 (June 27). However, quantities above 80 mm were verified in the SDY 20 (January 20) and closing the rainy season with records of 46.5 mm in the SDY 149 (May 29). As shown in Figure 5B, a significant amount of rainfall (53.7 mm) was registered on the sequential day of the year (SDY) 194 (July 13) at the INMET station in the region of Campina Grande-PB in which the CDeg and CRec towers are inserted.

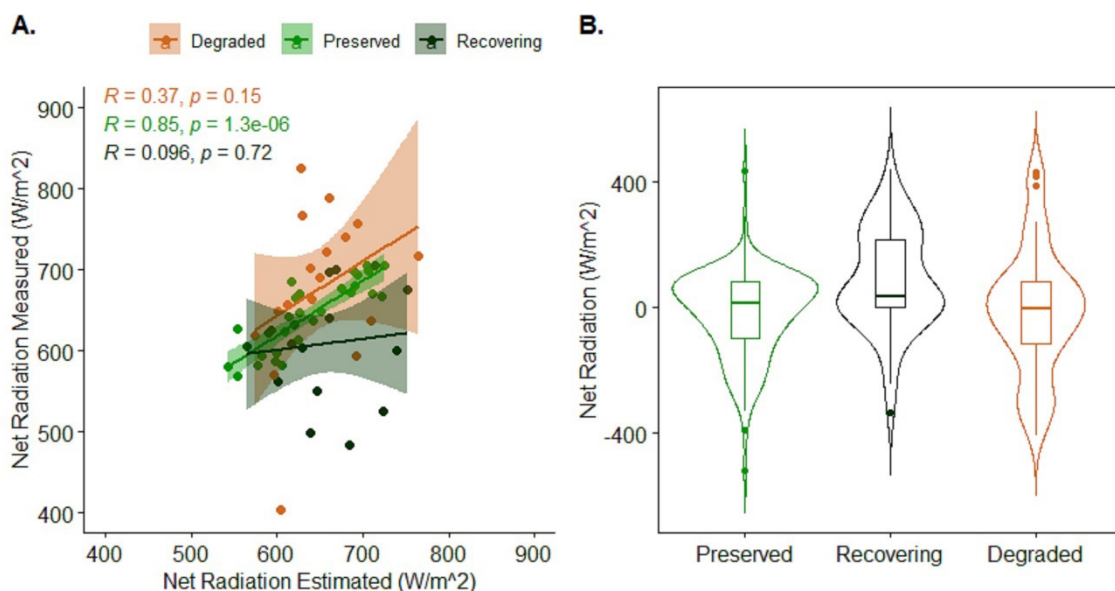


Figure 4 Distribution of the measured and estimated: A. Net radiation (Wm^{-2}) values in the studied areas; B. Associated absolute error.

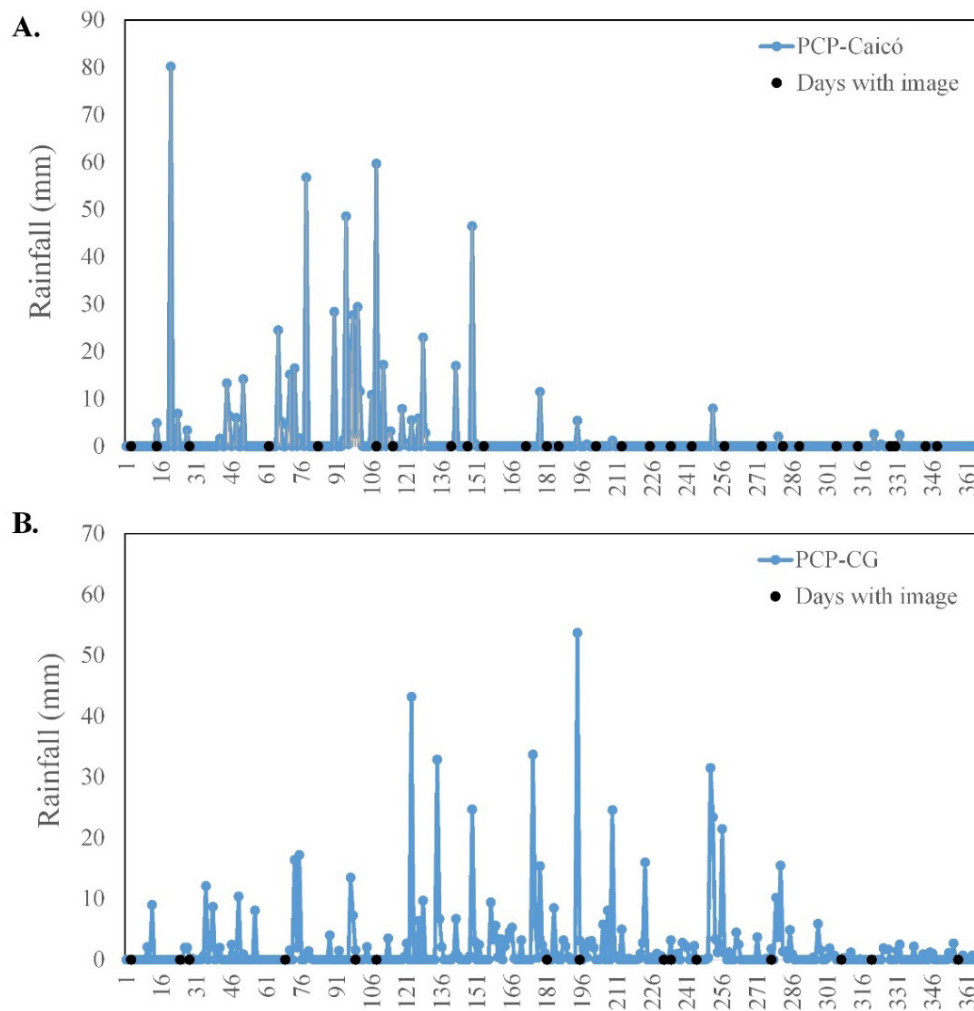


Figure 5 Daily rainfall distribution (mm) in 2014 according to the INMET meteorological station in the and records for the days with Terra MODIS images: A. Caicó-RN; B. Campina Grande-PB.

The energy available at the surface results from thermodynamic fluxes at the soil-plant-atmosphere interface, and degraded areas tend to have much higher surface temperatures than vegetated areas (Silva et al. 2014). However, in the current study, higher T_s values were found in CPres, either estimated through orbital images (316.6 K) or measured at micrometeorological towers (305.5 K). Values obtained through the two methods shown to be directly related (when one increased or decreased, the other showed similar behavior) (Figure 6A); however, increases were more sensitive in $T_{s(estimated)}$, while oscillation patterns of $T_{s(measured)}$ presented a lower amplitude. The pattern of overestimating T_s based on orbital images (i.e., $T_{s(estimated)} > T_{s(measured)}$ values) was frequent in the three areas studied; however, the estimated values below 305 K present good correspondence with observed values for the area of CPres.

According to AE statistics (Figure 6B), a mean error of 5 K was estimated for T_s . However, the amplitude of the AE was higher in CPres and lowered in CRec. The variability in energy availability and the conversion of R_n into distinct components of sensitive and latent fluxes can be excellent indications of the discrepant results obtained. Such results also reflect the importance of maintaining natural patterns in biomes such as Caatinga because of the effects of land cover changes on the adjacent environment.

3.3 Accuracy of the Estimates

Applications of orbital RS techniques, for example, in humid semiarid and tropical climates, are challenging. The main problem is the constant presence of clouds resulting from the convective process that is an important

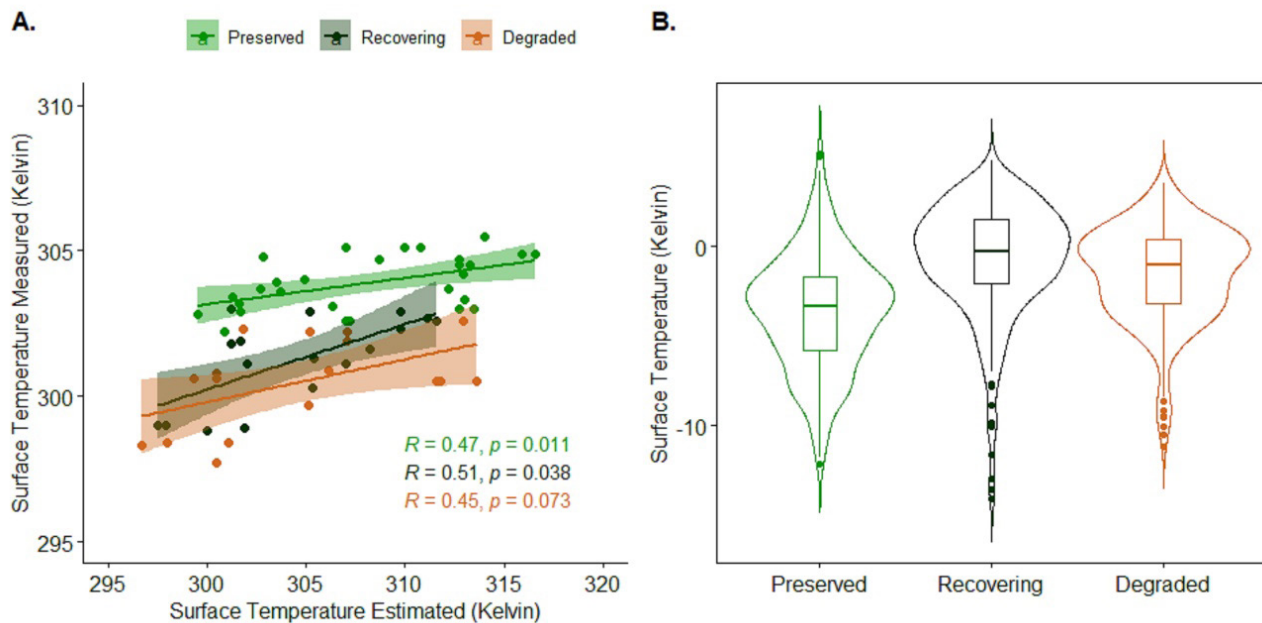


Figure 6 Distribution of measured and estimated: A. Surface temperature (Kelvin) values in the studied areas; B. Associated absolute error.

mechanism in heating the atmosphere in tropical regions (Santos et al. 2011). It is understood that the measured data are crucial to validate estimates from meteorological models because they are more realistic for a specific site. However, there are operational difficulties in their use; obtaining such measures requires a high financial investment, and they are usually limited to small areas and have no spatial representativity. Thus, RS represents an essential tool to document temporal and spatial variations of physical and biological characteristics of the surface, such as R_n , albedo, and normalized difference vegetation index (NDVI), thus improving the validations of parameterizations of physical-mathematical models used in environmental studies.

The quality of the estimates of environmental variables was demonstrated by the error statistics when the two-time series (measured versus estimated through the processing of MODIS digital products) were compared (Table 4) from January to December 2014. Regarding the cover patterns in CRec, CDeg and CPres, the results showed that albedo was the variable that presented the highest errors in the variables MAPE and NS. According to the MAPE values, the model used to estimate albedo was classified as inappropriate for CPres and CRec (> 25%) according to Liew et al. (2007), while it was classified as satisfactory for CDeg (15-25%). However, for the variable T_s , the MAPE

interval criteria indicated a very good fit of the model (<10%) for the three sites. It was also found that the NS showed a perfect fit for the variables R_n and T_s in CPres.

Still, regarding error statistics, it was identified in most analyses that the use of modeling using orbital products provided better performances of the d indices only for the adjustments to the observed data of the variable R_n in CPres (0.9) in comparison to the other observation points (CRec and CDeg).

Given the results of the error statistics, it was still necessary to compare the two sets of variables taking the median of the populations as a representative parameter. Thus, we used the Wilcoxon-Mann-Whitney non-parametric test in which the difference between ranks of the observations allows us to infer whether the estimated values are acceptable at a 5% level of significance. The results (Table 5) indicated that H_0 should be accepted only for R_n in the three observation sites; that is, a significant difference in practice was not detected. However, for albedo and T_s , p -values were less than or equal to the significance level, and thus H_1 was the alternative accepted. In practice, it is understood that there are differences in albedo and T_s values, and they are significant. Thus, we can conclude that the difference between the medians of the populations is statistically significant.

Table 4 Goodness-of-fit indicators for the analyzed variables at their respective data sample points.

| Locality/Variable | Goodness-of-fit indicator | | | | |
|------------------------------------|---------------------------|------|------|-------|------|
| | MAE | RMSE | MAPE | NS | d |
| Albedo (-) | | | | | |
| Preserved | 0.04 | 0.05 | 33.2 | -4.5 | 0.25 |
| Recovering | 0.1 | 0.1 | 53.7 | -67.7 | 0.1 |
| Degraded | 0.0 | 0.0 | 22.4 | -96.7 | 0.1 |
| R _n (Wm ⁻²) | | | | | |
| Preserved | 21.1 | 29.2 | 3.3 | 1.0 | 0.9 |
| Recovering | 67.0 | 91.6 | 12.1 | -1.0 | 0.5 |
| Degraded | 80.2 | 96.2 | 12.5 | 0.0 | 0.5 |
| Ts (K) | | | | | |
| Preserved | 5.2 | 6.4 | 1.7 | 1.0 | 0.3 |
| Recovering | 3.9 | 4.8 | 1.3 | -9.8 | 0.4 |
| Degraded | 4.7 | 6.3 | 1.5 | -16.6 | 0.3 |

Table 5 Wilcoxon-Mann-Whitney statistics at 5% level of significance for the data sample points.

| Locality (Caatinga) | Variable (p-value) | | |
|---------------------|--------------------|-----------------------------------|-------------------------|
| | Albedo (-) | Net radiation (Wm ⁻²) | Surface temperature (K) |
| Preserved | <0.0001*** | 0.71 | 0.006*** |
| Recovering | <0.0001*** | 0.08 | 0.05* |
| Degraded | 0.0002*** | 0.15 | 0.05* |

Significance codes: ***0.001, **0.01, *0.05.

4 Conclusions

The results derived from MODIS and validated with surface data proved to be satisfactory, relevant and efficient for use in environmental studies. However, location analyses in the use of data estimated by remote sensing are recommended to obtain coherent responses of temporal and spatial variations, especially when the surface characteristics are heterogeneous, thus helping to improve and validate parameterizations of physical-mathematical models. Significant differences between observed and estimated values were absent only for the variable R_n in the three observation sites. Therefore, we conclude that the R_n estimates obtained by processing orbital data were satisfactory for the three Caatinga coverage areas. These results are significant and can be used as tools for monitoring the process of surface energy exchange in semiarid regions.

5 Acknowledgments

The authors would like to thank the National Council for Scientific and Technological Development

(CNPq) for financing the Research Project under number 446172/2015-4; 409499/2018-8 and for providing a Research Productivity Grant (304493/2019-8) to the third author, as well as the Coordination for the Improvement of Higher Education Personnel (CAPES) for financing the Research Project entitled “Analysis and Prediction of Intense Hydrometeorological Phenomena in Eastern Northeast Brazil ”- Pro-Alertas Notice number 24/2014 (Process 88887.091737/2014-01).

6 References

- Allen, R.G., Pereira, L.S., Raes, D. & Smith, M. 1998, *Crop evapotranspiration: Guidelines for computing crop water requirements*, Paper No. 56, United Nations FAO, Irrigation and Drainage, New York.
- Allen, R., Tasumi, M. & Trezza, R. 2002, *SEBAL (Surface Energy Balance Algorithms for Land) – Advanced Training and User’s Manual– Idaho Implementation*, version 1.0, Idaho.
- Amatya, P.M., Ma, Y., Han, C., Wang, B. & Devkot, L. P. 2015, ‘Estimation of net radiation flux distribution on the southern slopes of the central Himalayas using MODIS data’, *Atmospheric Research*, vol. 154, pp. 146–54, DOI:10.1016/j.atmosres.2014.11.015.

- Araújo, A.L., Silva, M.T., Silva, B.B., Santos, C.A.C. & Amorim, M.R.B. 2017, 'Modelagem simplificada para estimativa do balanço de energia à superfície em escala regional (R-SSEB)', *Revista Brasileira de Meteorologia*, vol. 32, no. 3, pp. 433–46, DOI:10.1590/0102-77863230010.
- Araújo, A.L., Silva, M.T., Silva, B.B., Santos, C.A.C. & Dantas, M.P. 2018, 'Análise das mudanças de parâmetros biofísicos sobre o Nordeste Brasileiro de 2002 a 2011 com dados MODIS', *Revista Brasileira de Meteorologia*, vol. 33, no. 4, pp. 589–99, DOI:10.1590/0102-7786334002.
- Araújo, A.L., Silva, B.B. & Braga, C.C. 2012, 'Simplified modeling of downwelling long-wave radiation over Brazilian semi-arid under irrigation conditions', *Revista Brasileira de Geofísica*, vol. 30, no. 2, pp. 137–45, DOI:10.22564/rbfg.v30i2.87.
- Alvares, C.A., Stape, J.L., Sentelhas, P.C., Gonçalves, J.L.M. & Sparovek, G. 2014, 'Köppen's climate classification map for Brazil', *Meteorol. Z.*, vol. 22, no. 6, pp. 711–28, DOI:10.1127/0941-2948/2013/0507.
- Bastiaanssen, W.G.M. 1995, 'Regionalization of surface flux densities and moisture indicators in composite terrain: a remote sensing approach under clear skies in Mediterranean climates', PhD Dissertation, CIP Data Koninklijke Bibliotheek, Den Haag, The Netherlands.
- Bisht, G. & Bras, R.L. 2011, 'Estimation of net radiation from the moderate resolution imaging spectroradiometer over the continental United States', *IEEE Transactions on Geoscience and Remote Sensing*, vol. 49, no. 6, pp. 2448–62, DOI:10.1109/TGRS.2010.2096227.
- Bisht, G., Venturini, V., Islam, S. & Jiang, L. 2005, 'Estimation of the net radiation using MODIS (Moderate Resolution Imaging Spectroradiometer) data for clear-sky days', *Remote Sensing of Environment*, vol. 97, no. 1, pp. 52–67, DOI:10.1016/j.rse.2005.03.014.
- Carmona, F., Rivas, R. & Caselles, V. 2014, 'Estimation of daytime downward longwave radiation under clear and cloudy skies conditions over a sub-humid region', *Theoretical and Applied Climatology*, vol. 115, pp. 281–95, DOI:10.1007/s00704-013-0891-3.
- Ceballos, J.C., Bottino, M.J. & Souza, J.M.A. 2004, 'Simplified physical model for assessing solar radiation over Brazil using GOES 8 visible imagery', *Journal of Geophysical Research*, vol. 109, no. D2, D02211, DOI:10.1029/2003JD003531.
- Cochran, W.G. 1977, *Sampling techniques*, 3rd edn, John Wiley & Sons, New York.
- Cueto, R.G., Soto, N.S., Rincón, Z.H., Benítez, S.O. & Morales, G.B. 2015, 'Parameterization of net radiation in an arid city of northwestern Mexico', *Atmósfera*, vol. 28, no. 2, pp. 71–82, DOI:10.20937/ATM.2015.28.02.01.
- Duffie, J.A. & Beckman, W.A. 1991, *Solar engineering of thermal process*, 2nd edn, Wiley, New York.
- Francisco, P.R.M., Medeiros, R.M., Santos, D. & Matos, R.M. 2015, 'Classificação climática de Köppen e Thornthwaite para o estado da Paraíba', *Revista Brasileira de Geografia Física*, vol. 8, no. 4, pp. 1006–16, DOI:10.5935/1984-2295.20150049.
- Hwang, K., Choi, M., Lee, S.O. & Seo, J. 2013, 'Estimation of instantaneous and daily net radiation from MODIS data under clear sky conditions: a case study in East Asia', *Irrigation Science*, vol. 31, pp. 1173–84, DOI:10.1007/s00271-012-0396-3.
- Jiang, B., Zhang, Y., Liang, S., Wohlfahrt, G., Arain, A., Cescatti, A., Georgiadis, T., Jia, K., Kiely, G., Lund, M., Montagnani, L., Magliulo, V., Ortiz, P. S., Oechel, W., Vaccari, F.P., Yao, Y. & Zhang, X. 2015, 'Empirical estimation of daytime net radiation from shortwave radiation and ancillary information', *Agricultural and Forest Meteorology*, vol. 211–212, pp. 23–36, DOI:10.1016/j.agrformet.2015.05.003.
- Jiang, Y., Tang, R., Jiang, X. & Li, Z.-L. 2019, 'Impact of clouds on the estimation of daily evapotranspiration from MODIS-derived instantaneous evapotranspiration using the constant global shortwave radiation ratio method', *International Journal of Remote Sensing*, vol. 40, no. 5–6, pp. 1930–44, DOI:10.1080/01431161.2018.1482025.
- Liang, S.L., Wang, K.C., Zhang, X.T. & Wild, M. 2010, 'Review on estimation of land surface radiation and energy budgets from ground measurement, remote sensing and model simulations', *IEEE Journal of Selected Topics in Applied Earth Observations and Remote Sensing*, vol. 3, no. 3, pp. 225–40, DOI:10.1109/JSTARS.2010.2048556.
- Liew, M.W., Veith, T.L., Bosch, D.D. & Arnold, J.G. 2007, 'Suitability of SWAT for the Conservation effects assessment project: a comparison on USDA - ARS watersheds', *Journal of Hydrologic Engineering*, vol. 12, no. 2, pp. 173–89, DOI:10.1061/(ASCE)1084-0699(2007)12:2(173).
- Lu, J., Tang, R.L., Tang, H.J. & Li, Z.L. 2013, 'Derivation of daily evaporative fraction based on temporal variations in surface temperature, air temperature, and net radiation', *Remote Sensing*, vol. 5, no. 10, pp. 5369–96, DOI:10.3390/rs5105369.
- Mahalakshmi, D.V., Paul, A., Dutta, D., Ali, M.H., Reddy, R.S., Jha, C., Sharma, J.R. & Dadhwal, V.K. 2016, 'Estimation of net surface radiation from eddy flux tower measurements using artificial neural network for cloudy skies', *Sustainable Environment Research*, vol. 26, no. 1, pp. 44–50, DOI:10.1016/j.serj.2015.09.002.
- Marengo, J.A., Torres, R.R. & Alves, L.M. 2017, 'Drought in Northeast Brazil-past, present, and future', *Theoretical and Applied Climatology*, vol. 129, no. 3–4, pp. 1189–200, DOI:10.1007/s00704-016-1840-8.
- Marengo, J.A., Alves, L.M., Alvares, R.C.S., Cunha, A.P., Brito, S. & Moraes, O.L.L. 2018, 'Climatic characteristics of the 2010-2016 drought in the semi-arid Northeast Brazil region', *Anais da Academia Brasileira de Ciências*, vol. 90, no. 2, pp. 1973–85, DOI:10.1590/0001-3765201720170206.
- Marengo, J.A. & Bernasconi, M. 2015, 'Regional differences in aridity / drought conditions over Northeast Brazil: present state and future projections', *Climatic Change*, vol. 129, no. 1, pp. 103–15, DOI:10.1007/s10584-014-1310-1.
- Mira, M., Olioso, A., Gallego-Elvira, B., Courault, D., Garrigues, S., Marloie, O., Hagolle, O., Guillevic, P. & Boulet, G. 2016, 'Uncertainty assessment of surface net radiation derived from Landsat images', *Remote Sensing of Environment*, vol. 175, pp. 251–70, DOI:10.1016/j.rse.2015.12.054.
- Montgomery, D.C., Jennings, C.L. & Kulahci, M. 2015, *Introduction to time series analysis and forecasting*, 6th edn, Wiley-Interscience, New York.
- Nash, J.E. & Sutcliffe, J.V. 1970, 'River flow forecasting through conceptual models: a discussion of principles', *Journal of Hydrology*, vol. 10, no. 3, pp. 282–90, DOI:10.1016/0022-1694(70)90255-6.

- Oliveria, V.G., Silva, M.T., Santos, C.A.C., Serrão, E.A.O., Silva, B.K.N., Santos, M.R.S. & Corrêa, I.C.P. 2021, 'Variabilidade Temporal da Cobertura das Terras nos Estados da Paraíba e Rio Grande do Norte', *Revista Brasileira de Meteorologia*, vol. 36, no. 1, pp. 125–36, DOI:10.1590/0102-77863610011.
- Pigeon, G., Legain, D., Durand, P. & Masson, V. 2007, 'Anthropogenic heat release in an old European agglomeration (Toulouse, France)', *International Journal of Climatology*, vol. 27, no. 14, pp. 1969–81, DOI:10.1002/joc.1530.
- Pinker, R.T., Tarpley, J.D., Laszlo, I., Mitchell, K.E., Houser, P.R., Wood, E.F., Schaake, J.C., Robock, A., Lohmann, D., Cosgrove, B.A., Sheffield, J., Duan, Q., Luo, L. & Higgins, W. 2003, 'Surface radiation budgets in support of the GEWEX Continental-Scale International Project (GCIP) and the GEWEX Americas Prediction Project (GAPP), including the North American Land Data Assimilation System (NLDAS) project', *Journal of Geophysical Research Atmospheres*, vol. 108, no. D22, 8844, DOI:10.1029/2002JD003301.
- R Core Team 2016, *R: A language and environment for statistical computing*, *R Foundation for Statistical Computing*, Computer Program, viewed 12 December 2020, <<https://www.R-project.org/>>.
- Royston, J.B. 1983, 'Some techniques for assessing multivariate based on the Shapiro-Wilk W', *Journal of the Royal Statistical Society*, vol. 32, no. 2, pp. 121–33, DOI:10.2307/2347291.
- Santos, C.A.C., Silva, B.B., Rao, T.V.R., Satyamurti, P. & Manzi, A.O. 2011, 'Downward longwave radiation estimates for clear-sky conditions over Northeast Brazil', *Revista Brasileira de Meteorologia*, vol. 26, no. 3, pp. 443–50, DOI:10.1590/S0102-77862011000300010.
- Santos, C.A.C., Costa, M.V.G., Silva, M.T., Silva, L.L., Santos, F.A.C., Bezerra, B.G. & Medeiros, S.S. 2017, 'Obtenção de parâmetros ambientais na Região Semiárida da Paraíba por dados MODIS', *Revista Brasileira de Meteorologia*, vol. 32, no. 4, pp. 633–47, DOI:10.1590/0102-7786324011.
- Santos, F.A.C., Silva, B.B., Araújo, A.L., Silva, M.T. & Braga, A.C. 2013, 'Comparação de modelos de estimativa da radiação de onda curta a partir de dados MODIS/Terra', *Revista Brasileira de Geografia Física*, vol. 6, no. 4, pp. 1037–49, DOI:10.26848/rbgf.v6i5.233094.
- Santos, F.A.C., Santos, C.A.C., Silva, B.B., Araújo, A.L. & Cunha, J.E.B.L. 2015, 'Desempenho de metodologias para estimativa do saldo de radiação a partir de imagens MODIS', *Revista Brasileira de Meteorologia*, vol. 30, no. 3, pp. 295–306, DOI:10.1590/0102-778620130085.
- Santos, C.A.C., Mariano, D.A., Nascimento, F.C.A., Dantas, F.R.C., Oliveira, G., Silva, M.T., Silva, L.L., Silva, B.B., Bezerra, B.G., Safa, B., Medeiros, S.S. & Neale, C.M.U. 2020, 'Spatio-temporal patterns of energy exchange and evapotranspiration during an intense drought for drylands in Brazil', *International Journal of Applied Earth Observation and Geoinformation*, vol. 85, 101982, DOI:10.1016/j.jag.2019.101982.
- Silva, M.T., Silva, V.P.R., Silva, M.M.M.A., Silva, H.C.D. & Oliveira, N.F. 2014, 'Space time variability of surface temperature in the semi-arid Pernambuco based image TM/Landsat', *Journal of Hyperspectral Remote Sensing*, vol. 4, no. 4, pp. 111–20, DOI:10.29150/jhrs.v4.4.p111-120.
- Tasumi, M., Allen, R.G. & Trezza, R. 2008, 'At-surface reflectance and albedo from satellite for operational calculation of land surface energy balance', *Journal of Hydrologic Engineering*, vol. 13, no. 2, pp. 51–63, DOI:10.1061/(ASCE)1084-0699(2008)13:2(51).
- Tavares-Damasceno, J.P., Silveira, J.L.G.S., Camara, T., Stedile, P.C., Macario, P., Toledo-Lima, G.S. & Pichorim, M. 2017, 'Effect of drought on demography of Pileated Finch (*Coryphospingus pileatus*: Thraupidae) in northeastern Brazil', *Journal of Arid Environments*, vol. 147, pp. 63–70, DOI:10.1016/j.jaridenv.2017.09.006.
- Teixeira, A.H.C., Bastiaanssen, W.G.M., Ahmad, M.D., Moura, M.S.B. & Bos, M.G. 2008, 'Analysis of energy fluxes and vegetation-atmosphere parameters in irrigated and natural ecosystems of semi-arid Brazil', *Journal of Hydrology*, vol. 362, no. 1–2, pp. 110–27, DOI:10.1016/j.jhydrol.2008.08.011.
- Wang, T., Shi, J., Yu, Y., Husi, L., Gaob, B., Zhou, W., Ji, D., Zhao, T., Xiong, C. & Chenc, L. 2018, 'Cloudy-sky land surface longwave downward radiation (LWDR) estimation by integrating MODIS and AIRS/AMSU measurements', *Remote Sensing of Environment*, vol. 205, pp. 100–11, DOI:10.1016/j.rse.2017.11.011.

Author contributions

Madson Tavares Silva: conceptualization; formal analysis; methodology; validation; visualization; writing – original draft; writing – proofreading and editing. **Verônica Gabriella de Oliveira:** formal analysis; essay; original draft. **Carlos Antonio Costa dos Santos:** formal analysis; methodology; validation; visualization; writing – original draft. **Lindenberg Lucena da Silva:** Data collection; conceptualization; visualization. **Francineide Amorim Costa Santos:** formal analysis; methodology. **Edivaldo Afonso de Oliveira Serrão:** formal analysis; validation; visualization; writing – proofreading and editing

Conflict of interest

The authors have no potential conflicts of interest.

How to cite:

Silva, M.T., Oliveira, V.G., Santos, C.A.C., Silva, L.L., Santos, F.A.C. & Serrão, E.A.O. 2022, 'Net Radiation in the Semi-arid Region of the States of Paraíba and Rio Grande do Norte Using the MODIS Sensor', *Anuário do Instituto de Geociências*, 45:42790. https://doi.org/10.1137/1982-3908_45_42790

Data availability statement

All data included in this study are publicly available in literature.

Funding information

Research Project Grant 3033/2021, Paraíba State Research Foundation (FAPESQ).

Editor-in-chief

Dr. Claudine Dereczynski

Associate Editor

Dr. Renata Libonati